STRUCTURAL CONTROL AND HEALTH MONITORING
Struct. Control Health Monit. 2006; **13**:573–588
Published online 16 November 2005 in Wiley InterScience (www.interscience.wiley.com). DOI: 10.1002/stc.99

Smart base-isolated benchmark building. Part I: problem definition

S. Narasimhan[1], S. Nagarajaiah[2,*,†], E. A. Johnson[3] and H. P. Gavin[4]

[1] *Department of Civil and Environmental Engineering, Rice University, Houston, TX 77005, U.S.A.*
[2] *Department of Civil and Environmental Engineering and Mechanical Engineering and Material Science, Rice University, Houston, TX 77005, U.S.A.*
[3] *Department of Civil and Environmental Engineering, University of Southern California, Los Angeles, CA 90089, U.S.A.*
[4] *Department of Civil and Environmental Engineering, Duke University, Raleigh, Durham, NC 27708, U.S.A.*

SUMMARY

This paper presents the benchmark problem definition for seismically excited base-isolated buildings. The objective of this benchmark study is to provide a well-defined base-isolated building with a broad set of carefully chosen parameter sets, performance measures and guidelines to the participants, so that they can evaluate their control algorithms. The control algorithms may be passive, active or semi-active. The benchmark structure considered is an eight-storey base-isolated building similar to existing buildings in Los Angeles, California. The base isolation system includes both linear and nonlinear bearings and control devices. The superstructure is considered to be a linear elastic system with lateral–torsional behavior. A new nonlinear dynamic analysis program has been developed and made available to facilitate direct comparison of results of different control algorithms. Copyright © 2005 John Wiley & Sons, Ltd.

KEY WORDS: benchmark; base-isolated building; control

1. INTRODUCTION

Recently, well-defined analytical benchmark problems [1–6] have been developed for studying response control strategies for building and bridge structures subjected to seismic and wind excitation, by broad consensus effort of the ASCE structural control committee. The goal of this effort was to develop benchmark models to provide systematic and standardized means by which competing control strategies, including devices, algorithms, sensors, etc. can be evaluated. Carefully defined analytical benchmark problems are an excellent alternative to expensive experimental benchmark test structures. Due to effectiveness of the fixed base building benchmark effort [2–5], the ASCE structural control committee voted to develop a

*Correspondence to: Associate Professor S. Nagarajaiah, Department of Civil and Environmental Engineering and Mechanical Engineering and Material Science, Rice University, Houston, TX 77005, U.S.A.
† E-mail: nagaraja@rice.edu

Contract/grant sponsor: NSF, CAREER; contract/grant numbers: 99-96290, 00-94030

Received 9 September 2004
Revised 1 December 2004
Accepted 15 December 2004

new smart base-isolated benchmark problem. Narasimhan *et al.* [7–9] have developed the smart base-isolated benchmark problem, based on input from the ASCE structural control committee, with the capability to model three different kinds of base isolation systems: linear elastomeric systems with low damping or supplemental high damping; frictional systems; bilinear or nonlinear elastomeric systems, or any combination thereof. The superstructure is assumed to remain linear at all times. A host of control devices can be considered at the isolation level. No control devices are allowed in the superstructure.

Base isolation systems, such as sliding and elastomeric bearing systems, reduce the superstructure response, but with increased base displacements in near-fault motions. Current practice is to provide nonlinear passive dampers to limit the bearing displacements, however, this increases the forces in the superstructure and also at the isolation level. Active and semiactive devices present attractive alternatives to passive nonlinear devices. Active and semiactive control of linear and nonlinear structures using novel devices such as magnetorheological (MR) dampers, electrorheological dampers and variable stiffness systems has gained significant attention in the recent years [10]. The effectiveness of structural control strategies and different control algorithms has been demonstrated, by many researchers, experimentally and analytically [5, 10–14, 25, 26].

Participants of this benchmark study can propose control strategies for benchmark base-isolated building and define, evaluate, and report the results for the proposed strategy. A set of evaluation criteria have also been developed for the sake of comparison of various control strategies.

2. STRUCTURAL MODEL

The benchmark structure is a base-isolated eight-storey, steel-braced framed building, 82.4-m-long and 54.3-m-wide, similar to existing buildings in Los Angeles, California. The floor plan is L-shaped, as shown in Figure 1. The superstructure bracing is located at the building perimeter. Metal decking and a grid of steel beams support all concrete floor slabs. The steel superstructure is supported on a reinforced concrete base slab, which is integral with concrete beams below, and drop panels below each column location. The isolators are connected between these drop panels and the footings below, as shown in Figure 1. The superstructure is modeled as a three-dimensional linear elastic system. The superstructure members, such as beam, column, bracing, and floor slab are modeled in detail. Floor slabs and the base are assumed to be rigid in plane. The superstructure and the base are modeled using three master degrees of freedom (DOF) per floor at the center of mass. The combined model of the superstructure (24 DOF) and isolation system (3 DOF) consists of 27 degrees of freedom. All twenty four modes in the fixed-base case are used in modeling the superstructure. The superstructure damping ratio is assumed to be 5% in all fixed-base modes.

The computed natural periods for all 24 fixed-base modes are shown in Table I. The nominal isolation system consists of 61 friction pendulum bearings and 31 linear elastomeric bearings, as shown in Figure 1. The nominal isolation system can also be regarded as a linear isolation system consisting of 92 linear elastomeric bearings and 61 passive friction dampers; since, the friction pendulum bearings consists of an linear elastic part due to the curvature of the sliding

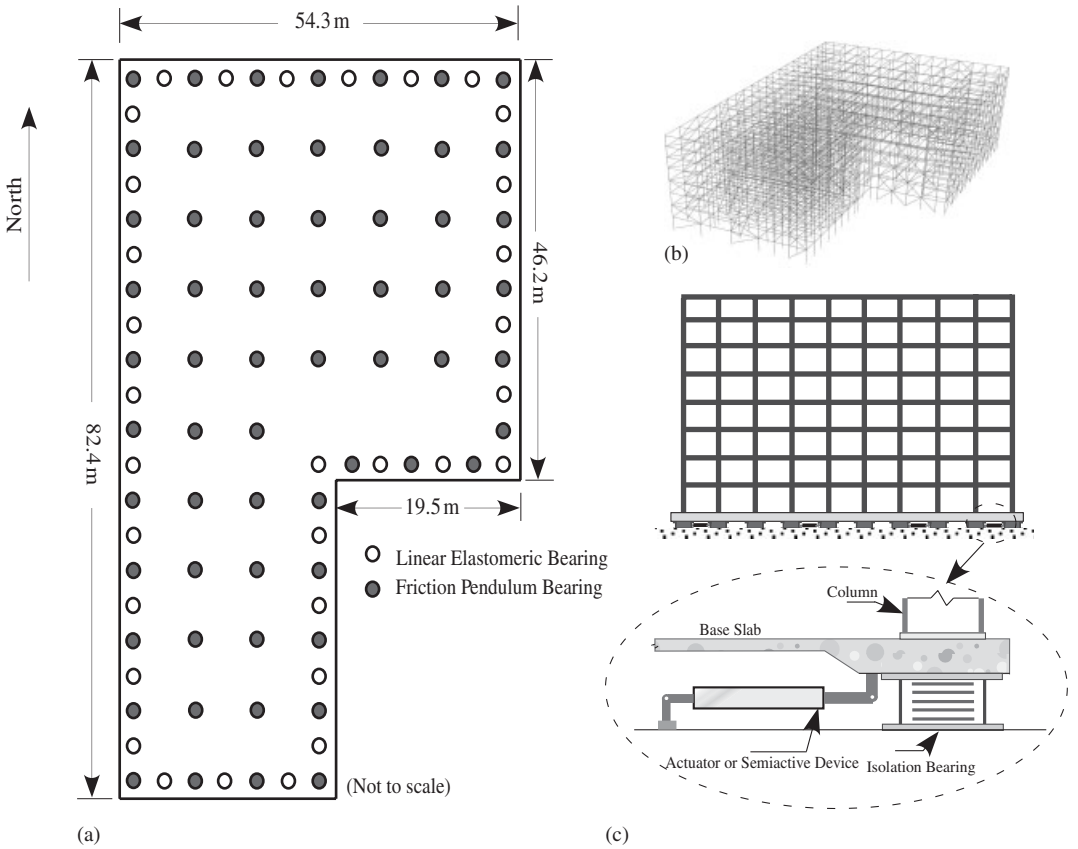

Figure 1. (a) Isolation plan; (b) FEM model of superstructure; and (c) elevation view with devices.

Table I. Periods of the superstructure.

	North–South	East–West	Torsion
1	0.78	0.89	0.66
2	0.27	0.28	0.21
3	0.15	0.15	0.12
4	0.11	0.11	0.08
5	0.08	0.08	0.07
6	0.07	0.07	0.06
7	0.06	0.06	0.06
8	0.05	0.06	0.05

surface and friction. While the nominal model contains sliding and linear elastomeric bearings, participants may replace them with other types of bearings. The total weight of the structure is 202 000 kN.

3. ISOLATION MODEL

Several isolation elements are included so that any combination of these can be used to model the isolation system completely. The isolation elements are elastic, viscous, hysteretic elements for bilinear elastomeric bearings and hysteretic elements for sliding bearings. The force–displacement characteristics for friction pendulum, lead rubber bearing and linear isolation bearings are shown in Figure 2. The hysteretic elements can be uniaxial or biaxial. The linear elastic and viscous elements are for modeling linear elastomeric bearings and fluid dampers. They can also be used for modeling bilinear elastomeric isolation systems with corresponding equivalent linear properties, obtained using appropriate linearization techniques.

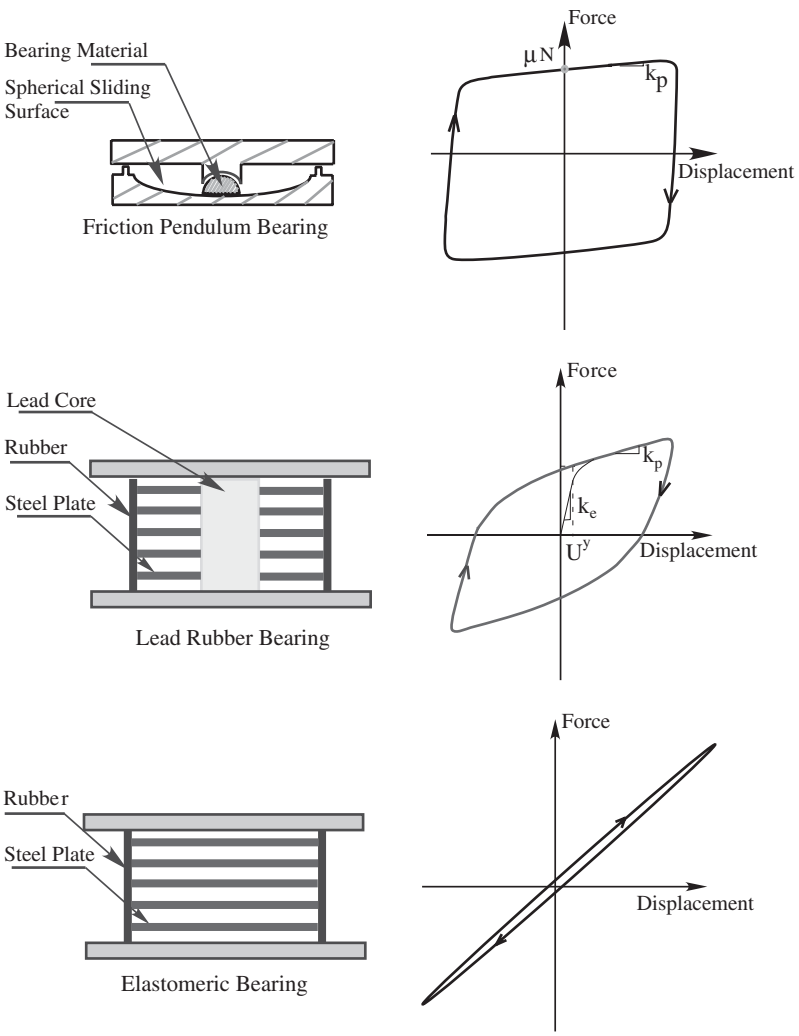

Figure 2. Force–displacement characteristics of bearings.

The biaxial hysteretic behavior of bilinear elastomeric bearings and/or frictional bearings is modeled using the biaxial interaction equations of Bouc–Wen model [15] as follows:

$$U^y \begin{Bmatrix} \dot{z}_x \\ \dot{z}_y \end{Bmatrix} = \alpha \begin{Bmatrix} \dot{U}_x \\ \dot{U}_y \end{Bmatrix} - \mathbf{Z}_w \begin{Bmatrix} \dot{U}_x \\ \dot{U}_y \end{Bmatrix}$$

$$\mathbf{Z}_w = \begin{bmatrix} z_x^2(\gamma sgn(\dot{U}_x z_x) + \beta) & z_x z_y(\gamma sgn(\dot{U}_y z_y) + \beta) \\ z_x z_y(\gamma sgn(\dot{U}_x z_x) + \beta) & z_y^2(\gamma sgn(\dot{U}_y z_y) + \beta) \end{bmatrix} \tag{1}$$

where z_x and z_y are dimensionless hysteretic variables that are bounded by values ± 1, α, β and γ are dimensionless quantities, U_x, U_y and $\dot{U}_x$, $\dot{U}_y$, represent the displacements and velocities in the x and y directions, respectively, at the isolation bearing or device and U^y is the yield displacement. Equation (1) accounts for biaxial interaction of both sliding and bilinear hysteretic bearings. When yielding commences Equation (1) leads to $z_x = \cos\theta$ and $z_y = \sin\theta$ provided $\alpha/(\beta + \gamma) = 1$ with $\theta = \tan^{-1}(\dot{U}_x/\dot{U}_y)$ and resultant velocity $\dot{U} = \sqrt{\dot{U}_x^2 + \dot{U}_y^2}$. The biaxial interaction can be neglected when the off-diagonal terms of the matrix in Equation (1) are replaced by zeros. This results in uniaxial model with two independent elements in two orthogonal directions.

The forces, f, mobilized in the elastomeric isolation bearings or devices can be modeled by a elastic–viscoplastic model with strain hardening

$$f_x = k_p U_x + c_v \dot{U}_x + (k_e - k_p) U^y z_x \tag{2}$$

$$f_y = k_p U_y + c_v \dot{U}_y + (k_e - k_p) U^y z_y \tag{3}$$

where k_e = pre-yield stiffness, k_p = post-yield stiffness, c_v = viscous damping coefficient of the elastomeric bearing or device, U^y is the yield displacement.

Equation (1) can also be used to model sliding bearings with flat or spherical sliding surface, by means of a small yield displacement U^y (because of rigid plastic behavior and large pre-yield stiffness) setting $c_v = 0$ and $(k_e - k_p)\ U^y = \mu N$

$$f_x = k_p U_x + \mu N z_x \tag{4}$$

$$f_y = k_p U_y + \mu N z_y \tag{5}$$

where μ is the coefficient of friction and N is the average normal force at the bearing (normal force variation is neglected). In Equations (4) and (5), the terms $k_p U_x$ and $k_p U_y$ represent the re-centering force due to the spherical surface of a friction pendulum bearing or a flat slider. In a similar manner other devices such as nonlinear fluid dampers can also be modeled using Equation (1).

The nominal isolation system consists of 61 friction pendulum bearings (or 61 linear bearings and 61 friction dampers) and 31 linear elastomeric bearings; however, the participants may replace them with other types of bearings. Three types of base isolation systems are considered for control design purposes: (1) linear elastomeric isolation system with low damping; (2) nonlinear friction isolation system representing friction pendulum system; and (3) bilinear

elastomeric isolation system representing a lead–rubber system. The isolation systems and the corresponding sample control designs have been described in detail in companion papers [16–18].

In phase I, the participants can compare the results of their controllers with the results of the sample active and semiactive controllers presented by Nagarajaiah and Narasimhan [17] for the nominal linear isolation system. Additionally, they may also compare the results of their controllers with a preliminary skyhook controller presented by Nagarajaiah and Narasimhan [17]. They may also compare their passive design with the work of Alhan and Gavin [19].

4. THREE-DIMENSIONAL NONLINEAR DYNAMIC ANALYSIS

Base-isolated buildings are designed such that the superstructure remains elastic. Hence, in this study the superstructure is modeled by a condensed linear elastic system. Also, the localized nonlinearities at the isolation level allow condensation of the linear superstructure. In addition, the equations of motion are developed in such a way that the fixed-base properties are used for modeling the linear superstructure. The base and the floors are assumed to be infinitely rigid in plane. The superstructure and the base are modeled using three master degrees of freedom (DOF) per floor at the center of mass. Each nonlinear isolation bearing or device is modeled explicitly using the discrete biaxial Bouc–Wen model, and the forces in the bearings or devices are transformed to the center of mass of the base using a rigid base slab assumption. All the linear isolation bearings or devices can be modeled individually or globally by equivalent lumped elements at the center of mass of the base. The displacement coordinates are shown in Figure 3 and the asymmetric model is shown in Figure 4. The equations of motion for the elastic superstructure are expressed in the following form:

$$\mathbf{M}_{n\times n}\ddot{\mathbf{U}}_{n\times 1} + \mathbf{C}_{n\times n}\dot{\mathbf{U}}_{n\times 1} + \mathbf{K}_{n\times n}\mathbf{U}_{n\times 1} = -\mathbf{M}_{n\times n}\mathbf{R}_{n\times 3}(\ddot{\mathbf{U}}_{\mathrm{g}} + \ddot{\mathbf{U}}_{\mathrm{b}})_{3\times 1} \tag{6}$$

in which, n is three times the number of floors (excluding base), $\mathbf{M}$ is the superstructure mass matrix, $\mathbf{C}$ is the superstructure damping matrix in the fixed-base case, $\mathbf{K}$ is the superstructure stiffness matrix in the fixed-base case and $\mathbf{R}$ is the matrix of earthquake influence coefficients, i.e. the matrix of displacements and rotation at the center of mass of the floors resulting from a unit translation in the X and Y directions and unit rotation at the center of mass of the base. Furthermore, $\ddot{\mathbf{U}}$, $\dot{\mathbf{U}}$ and $\mathbf{U}$ represent the floor acceleration, velocity and displacement vectors relative to the base, $\ddot{\mathbf{U}}_{\mathrm{b}}$ is the vector of base accelerations relative to the ground and $\ddot{\mathbf{U}}_{\mathrm{g}}$ is the vector of ground accelerations. The control devices are located at the isolation level only as shown in Figure 1. The equations of motion for the base are as follows:

$$\begin{aligned}\mathbf{R}^{\mathrm{T}}_{3\times n}\mathbf{M}_{n\times n}[(\ddot{\mathbf{U}})_{n\times 1} + \mathbf{R}_{n\times 3}(\ddot{\mathbf{U}}_{\mathrm{g}} + \ddot{\mathbf{U}}_{\mathrm{b}})_{3\times 1}]_{n\times 1} + \mathbf{M}_{\mathrm{b}_{3\times 3}}(\ddot{\mathbf{U}}_{\mathrm{g}} + \ddot{\mathbf{U}}_{\mathrm{b}})_{3\times 1} + \mathbf{C}_{\mathrm{b}_{3\times 3}}\dot{\mathbf{U}}_{\mathrm{b}_{3\times 1}} \\ + \mathbf{K}_{\mathrm{b}_{3\times 3}}\mathbf{U}_{\mathrm{b}_{3\times 1}} + \mathbf{f}_{\mathrm{B}_{3\times 1}} + \mathbf{f}_{\mathrm{c}_{3\times 1}} = 0\end{aligned} \tag{7}$$

in which $\mathbf{M}_{\mathrm{b}}$ is the diagonal mass matrix of the rigid base, $\mathbf{C}_{\mathrm{b}}$ is the resultant damping matrix of viscous isolation elements, $\mathbf{K}_{\mathrm{b}}$ is the resultant stiffness matrix of elastic isolation elements, $\mathbf{f}_{\mathrm{B}}$ is the vector containing the nonlinear bearing forces and $\mathbf{f}_{\mathrm{c}}$ is the vector containing the control forces. Equation (6) can be reformulated in the modal domain and the fixed-base frequencies, damping ratios, and modes can be used for modeling the superstructure [20, 21]. Using

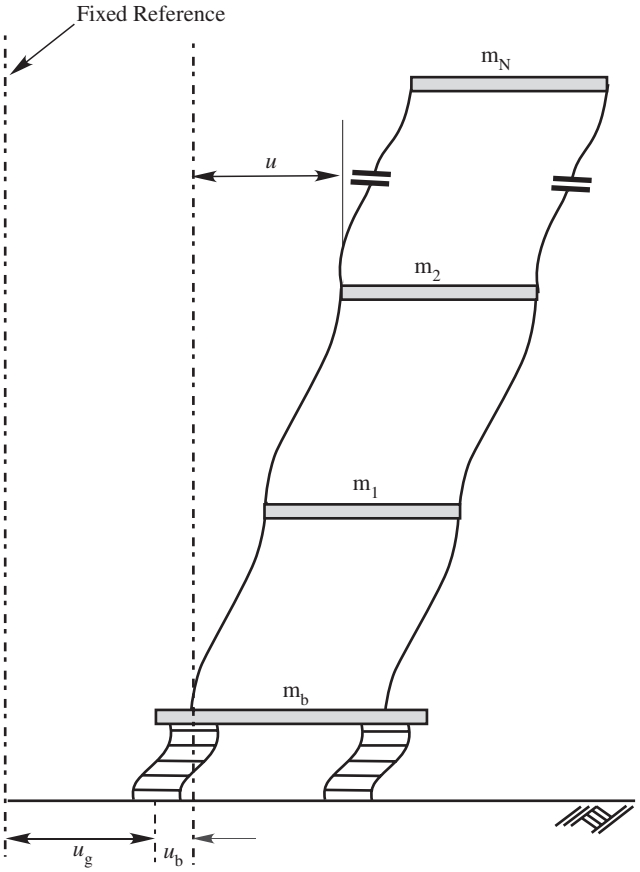

Figure 3. Displacement coordinates of the base-isolated structure.

$\mathbf{X} = \{\mathbf{U}^{\mathrm{T}}\ \mathbf{U}_{\mathrm{b}}^{\mathrm{T}}\ \dot{\mathbf{U}}^{\mathrm{T}}\ \dot{\mathbf{U}}_{\mathrm{b}}^{\mathrm{T}}\}^{\mathrm{T}}$, the state space equations can be formulated as

$$\dot{\mathbf{X}}(t) = \mathbf{A}\mathbf{X}(t) + \mathbf{B}\mathbf{u}(t) + \mathbf{B}^{*}\mathbf{F}_{\mathrm{B}}(t) + \mathbf{E}\ddot{\mathbf{U}}_{\mathrm{g}}(t) = \mathbf{g}(\mathbf{X}, \mathbf{u}, \ddot{\mathbf{U}}_{\mathrm{g}}) \tag{8}$$

$$\mathbf{A} = \begin{bmatrix} \mathbf{0} & \mathbf{I} \\ -\bar{\mathbf{M}}^{-1}\bar{\mathbf{K}} & -\bar{\mathbf{M}}^{-1}\bar{\mathbf{C}} \end{bmatrix} \qquad \mathbf{E} = \begin{bmatrix} \mathbf{0} \\ -\bar{\mathbf{M}}^{-1} \begin{Bmatrix} \mathbf{MR} \\ \mathbf{R}^{\mathrm{T}}\mathbf{MR} + \mathbf{M}_{\mathrm{b}} \end{Bmatrix} \end{bmatrix}$$

$$\mathbf{B} = \mathbf{B}^{*} = \begin{bmatrix} \mathbf{0} \\ -\bar{\mathbf{M}}^{-1} \begin{Bmatrix} \mathbf{0} \\ \mathbf{I} \end{Bmatrix} \end{bmatrix}$$

$$\bar{\mathbf{M}} = \begin{bmatrix} \mathbf{M} & \mathbf{MR} \\ \mathbf{R}^{\mathrm{T}}\mathbf{M} & \mathbf{R}^{\mathrm{T}}\mathbf{MR} + \mathbf{M}_{\mathrm{b}} \end{bmatrix} \qquad \bar{\mathbf{C}} = \begin{bmatrix} \mathbf{C} & \mathbf{0} \\ \mathbf{0} & \mathbf{C}_{\mathrm{b}} \end{bmatrix}$$

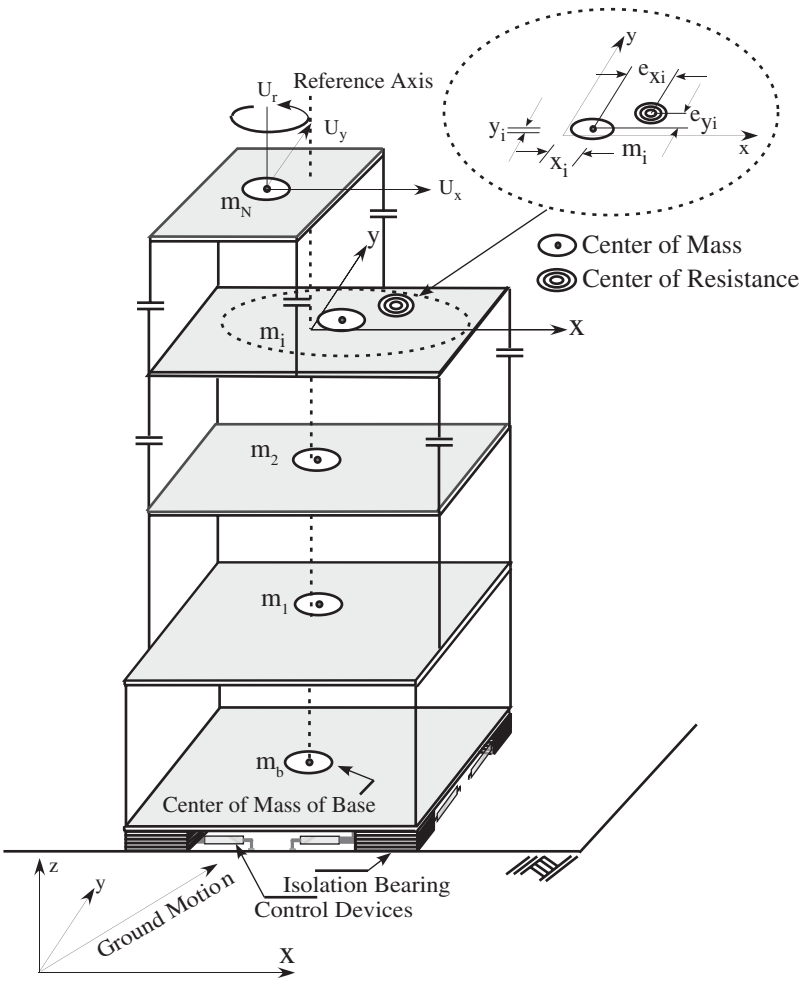

Figure 4. Asymmetric base-isolated structure excited by bidirectional ground motion.

$$\bar{\mathbf{K}} = \begin{bmatrix} \mathbf{K} & \mathbf{0} \\ \mathbf{0} & \mathbf{K}_b \end{bmatrix} \qquad \mathbf{u} = \begin{bmatrix} \mathbf{0} \\ \mathbf{f}_c \end{bmatrix} \qquad \mathbf{F}_B = \begin{bmatrix} \mathbf{0} \\ \mathbf{f}_B \end{bmatrix}$$

In these equations, **A**, **B**, **B*** and **E** are condensed system matrices having 54 states derived from the full three-dimensional finite element model. Equation (8) is solved using Newmark's unconditionally stable constant-average acceleration method, which can also be derived from the trapezoidal rule given by

$$\mathbf{X}_{k+1} = \mathbf{X}_k + \frac{\Delta t}{2}(\mathbf{g}_k + \mathbf{g}_{k+1}) \tag{9}$$

where $\mathbf{g}_{k+1} = \mathbf{g}(\mathbf{X}_{k+1}, \mathbf{u}_{k+1}, \ddot{\mathbf{U}}_{g_{(k+1)}})$. This method is implicit, needing iteration. The nonlinear forces in the isolation bearings, devices and control forces are updated by solving Equations (1)–(5) using the unconditionally stable semi-implicit Runge–Kutta method [22] suitable for

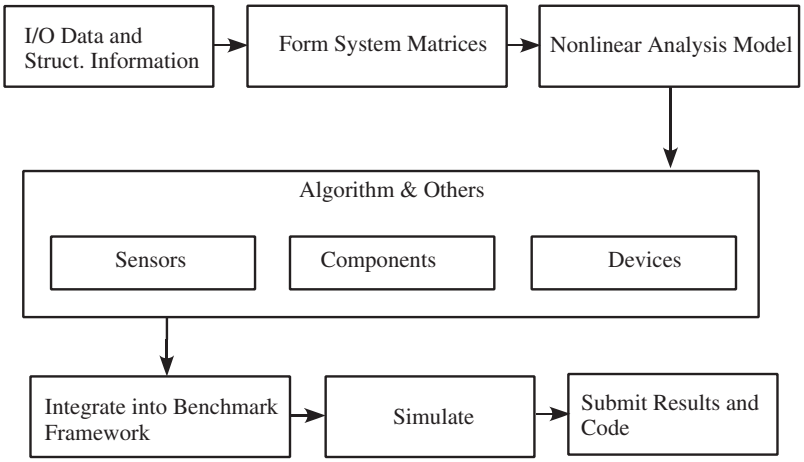

Figure 5. Schematics of MATLAB/SIMULINK implementation.

solutions of stiff differential equations. Then Equation (8) is resolved using an iterative predictor–corrector solution procedure [20, 21] until equilibrium of nonlinear forces is reached within specified tolerance and convergence is achieved.

5. MATLAB IMPLEMENTATION

The analytical model is implemented using MATLAB [24] and SIMULINK [24] as shown in Figure 5. The analysis program uses an input data file, a file to read and assemble the required matrices for input into the nonlinear dynamic analysis block, which is a SIMULINK based S-function program. The full implementation procedure is shown in Figure 6. Additional inputs to the nonlinear analysis block are the seismic excitation and the control forces provided by the control devices. The nonlinear response is calculated using a predictor–corrector algorithm as explained in the earlier sections. All sensor and control devices can be modeled in this program as SIMULINK blocks and the outputs of these models fed into the analysis S-function block.

6. CONTROL DESIGN

The benchmark study participants are to define the type, appropriate model, and location of the sensor(s), control devices, and control algorithms (see Figure 5). The analysis program will remain invariant to the various control strategies developed and implemented. The various control strategies can be compared with one another by having the model and evaluation criteria common to all controllers. The control devices, sensor devices and the control algorithms can be interfaced to the structural evaluation model through measurement and device connection outputs, designated $\mathbf{y}_m$ and $\mathbf{y}_{cd}$ respectively. The evaluation outputs $\mathbf{y}_e$ are used for the calculation of performance indices. The outputs $\mathbf{y}_m$ and $\mathbf{y}_{cd}$ are specified in the input files provided with the benchmark problem statement.

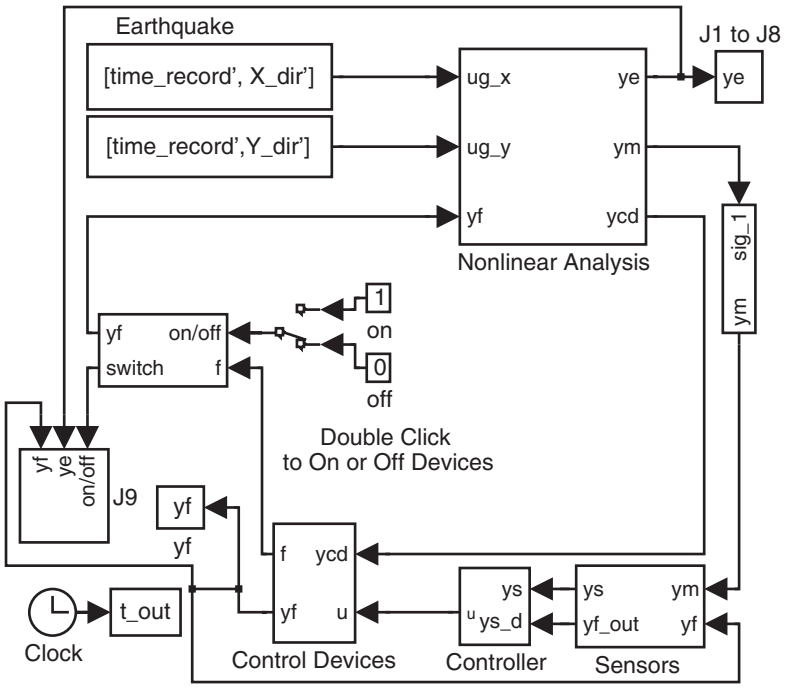

Figure 6. SIMULINK block diagram for simulations.

6.1. Sensor models

The sensors must take the following form

$$\dot{\mathbf{X}}^{\mathrm{s}} = \mathbf{g}_1(\mathbf{X}^{\mathrm{s}}, \mathbf{y}_{\mathrm{m}}, \mathbf{u}_{\mathrm{m}}, \mathbf{t}) \tag{10}$$

$$\mathbf{y}^{\mathrm{s}} = \mathbf{g}_2(\mathbf{X}^{\mathrm{s}}, \mathbf{y}_{\mathrm{m}}, \mathbf{u}_{\mathrm{m}}, \mathbf{v}, \mathbf{t}) \tag{11}$$

where $\mathbf{X}^{\mathrm{s}}$ are the states of the sensor, $\mathbf{v}$ is the measurement noise vector, $\mathbf{u}_{\mathrm{m}}$ is a vector of control device continuous time responses and $\mathbf{y}^{\mathrm{s}}$ is the output of the sensor in units of volts (Figure 7). $\mathbf{u}_{\mathrm{m}}$ may consist of device forces and/or stroke that may be needed for feedback into the controller.

6.2. Control algorithm

Control algorithms may be designed to work with active or semiactive systems. The discrete form of the control algorithms may be written as

$$\mathbf{X}^{\mathrm{c}}_{k+1} = \mathbf{g}_3(\mathbf{X}^{\mathrm{c}}_k, \mathbf{y}^{\mathrm{s}}_k, \mathbf{k}) \tag{12}$$

$$\mathbf{u}_k = \mathbf{g}_4(\mathbf{X}^{\mathrm{c}}_k, \mathbf{y}^{\mathrm{s}}_k, \mathbf{k}) \tag{13}$$

where $\mathbf{X}^{\mathrm{c}}_k$ is the discrete state vector at time $t = \mathbf{k}\Delta t$, $\mathbf{y}^{\mathrm{s}}_k$ is the discretized sensor model output and $\mathbf{u}_k$ is the discrete control command from the control algorithm (Figure 8).

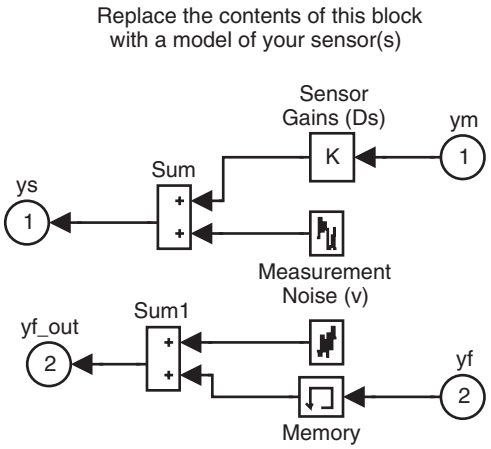

Figure 7. Sensor model implementation.

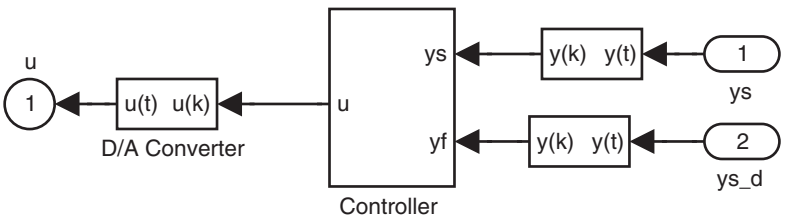

Figure 8. Control algorithm implementation.

6.3. Control devices

Control devices may be designed neglecting the dynamics of the devices, although including device dynamics is strongly encouraged. Control devices may only be placed at the isolation level and their possible locations are specified in the input files provided with the benchmark problem statement. The device models can be interfaced with the building model by including the dynamics of the device (Figure 9) as follows

$$\dot{\mathbf{X}}^{\mathrm{cd}} = \mathbf{g}_5(\mathbf{X}^{\mathrm{cd}}, \mathbf{y}_{\mathrm{cd}}, \mathbf{u}_k, \mathbf{t}) \tag{14}$$

$$\mathbf{u} = \mathbf{g}_6(\mathbf{X}^{\mathrm{cd}}, \mathbf{y}_{\mathrm{cd}}, \mathbf{u}_k, \mathbf{t}) \tag{15}$$

$$\mathbf{y}_{\mathrm{f}} = \mathbf{g}_7(\mathbf{X}^{\mathrm{cd}}, \mathbf{y}_{\mathrm{cd}}, \mathbf{u}_k, \mathbf{t}) \tag{16}$$

where the continuous states of the devices are represented by $\mathbf{X}^{\mathrm{cd}}$. If the dynamics are neglected, then the model is

$$\mathbf{u} = \mathbf{g}_8(\mathbf{y}_{\mathrm{cd}}, \mathbf{u}_k, \mathbf{t}) \tag{17}$$

$$\mathbf{y}_{\mathrm{f}} = \mathbf{g}_9(\mathbf{y}_{\mathrm{cd}}, \mathbf{u}_k, \mathbf{t}) \tag{18}$$

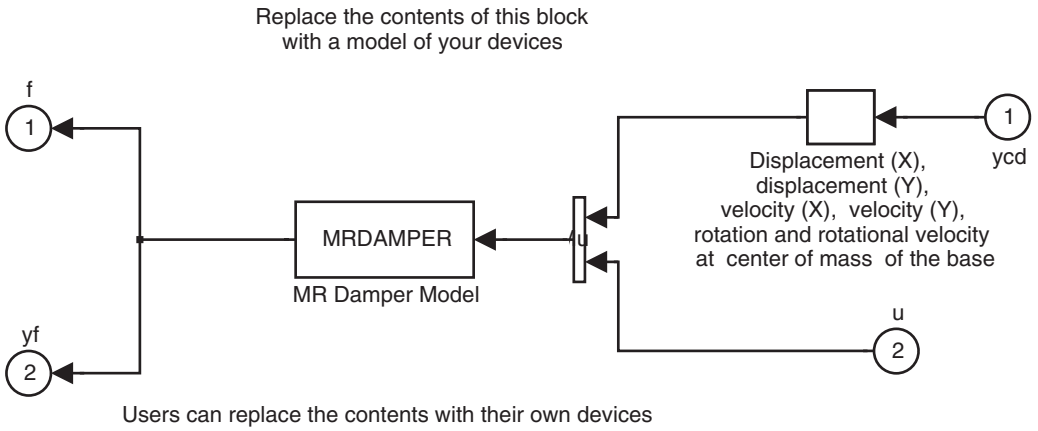

Figure 9. Control devices implementation.

7. EVALUATION CRITERIA

The following nine evaluation criteria are defined for the benchmark problem based on both maximum and RMS responses of the building. For each control design, these criteria must be evaluated for all seven earthquakes, in two orthogonal directions. In the following discussion, the term 'uncontrolled' refers to the isolation system containing linear and nonlinear bearings, but with no supplemental passive dampers or control devices.

1. Peak base shear (isolation-level) in the controlled structure normalized by the corresponding shear in the uncontrolled structure

$$J_1(q) = \frac{\max_t \|V_0(t,q)\|}{\max_t \|\hat{V}_0(t,q)\|}$$

2. Peak structure shear (at first storey level) in the controlled structure normalized by the corresponding shear in the uncontrolled structure

$$J_2(q) = \frac{\max_t \|V_1(t,q)\|}{\max_t \|\hat{V}_1(t,q)\|}$$

3. Peak base displacement or isolator deformation in the controlled structure normalized by the corresponding displacement in the uncontrolled structure

$$J_3(q) = \frac{\max_{t,i} \|d_i(t,q)\|}{\max_{t,i} \|\hat{d}_i(t,q)\|}$$

4. Peak inter-storey drift in the controlled structure normalized by the corresponding inter-storey drift in the uncontrolled structure

$$J_4(q) = \frac{\max_{t,f} \|d_f(t,q)\|}{\max_{t,f} \|\hat{d}_f(t,q)\|}$$

5. Peak absolute floor acceleration in the controlled structure normalized by the corresponding acceleration in the uncontrolled structure

$$J_5(q) = \frac{\max_{t,f} \|a_f(t,q)\|}{\max_{t,f} \|\hat{a}_f(t,q)\|}$$

6. Peak force generated by all control devices normalized by the peak base shear in the controlled structure

$$J_6(q) = \frac{\max_t \| \sum_k F_k(t,q)\|}{\max_t \|V_0(t,q)\|}$$

7. RMS base displacement in the controlled structure normalized by the corresponding RMS base displacement in the uncontrolled structure

$$J_7(q) = \frac{\max_i \|\sigma_d(t,q)\|}{\max_i \|\sigma_{\hat{d}}(t,q)\|}$$

8. RMS absolute floor acceleration in the controlled structure normalized by the corresponding RMS acceleration in the uncontrolled structure

$$J_8(q) = \frac{\max_f \|\sigma_a(t,q)\|}{\max_f \|\sigma_{\hat{a}}(t,q)\|}$$

9. Total energy absorbed by all control devices normalized by energy input into the controlled structure

$$J_9(q) = \frac{\sum_k \left[\int_0^{T_q} F_k(t,q) v_k(t,q)\, \mathrm{d}t \right]}{\int_0^{T_q} \langle V_0(t,q) \dot{U}_g(t,q) \rangle\, \mathrm{d}t}$$

where, $i =$ isolator number, $1, \ldots, N_i$ ($N_i = 8$); $k =$ device number, $1, \ldots, N_d$; $f =$ floor number, $1, \ldots, N_f$; $q =$ earthquake number: $1, \ldots, 5$; $t =$ time, $0 \leqslant t \leqslant T_q$; $\langle \cdot \rangle =$ inner product; $\| \cdot \| =$ vector magnitude incorporating NS and EW components.

8. EARTHQUAKES

The earthquakes used in this study are both the fault-normal (FN) and fault-parallel (FP) components of Newhall, Sylmar, El Centro, Rinaldi, Kobe, Ji-ji and Erzinkan as shown in Figure 10. All the excitations are used at the full intensity for the evaluation of the performance indices.

9. CONTROL IMPLEMENTATION AND RESTRICTIONS

1. The outputs that are available for direct measurement are the absolute accelerations at the center of mass of all floor levels and the base. The absolute accelerations consist of two translational and one rotational direction at each level. In addition, the absolute accelerations and relative displacements at all device locations in two translational directions and the ground accelerations are available for measurement. Absolute velocity measurements may be added by passing the measured accelerations through an appropriate second order filter [2, 3].

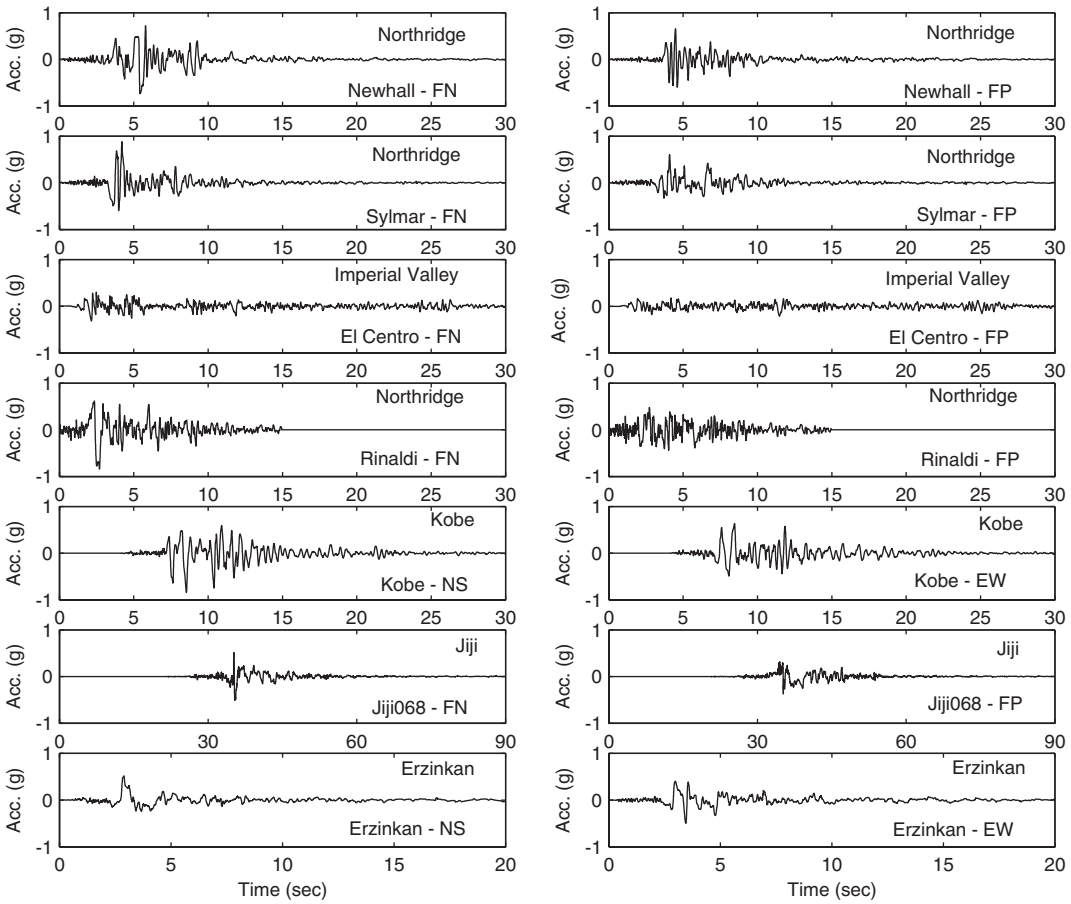

Figure 10. Time-histories of earthquake records. FP fault Parallel; FN fault Normal; EW East–West; NS North–South.

2. The digitally implemented controller should have a sampling time between 0.001 and 0.01 s.
3. The A/D and D/A converters for the digital controller have a 16-bit precision and a span of ± 10 V.
4. Small RMS noise (at least 0.05 V) should be added to the measured outputs.
5. All control devices should be placed only at the isolation level and no provision is made for their placement in the superstructure. A maximum of ninety-two control devices in the x-direction and another ninety-two control devices in the y-direction can be placed at the bearing locations.
6. The designer of the controller must justify that the proposed algorithm can be implemented with the existing hardware and computational resources.
7. The control algorithm has to be stable and closed-loop stability has to be ensured.
8. The algorithm must be implemented for all seven earthquakes provided (i.e. Newhall, Sylmar, El Centro, Rinaldi, Kobe, Ji-ji and Erzinkan) and results presented in terms of the performance indices in each direction of the excitation considered.

9. The isolation type and parameters can be changed as per the designer's requirement. However, their locations and total number in the building are fixed (a total of 92 bearings).
10. The maximum total force generated by the control devices in each direction must be less than or equal to the maximum total nonlinear or/and linear forces generated by the uncontrolled isolation system, i.e. the maximum total force in the controlled isolation system cannot exceed twice that of the maximum total force in the uncontrolled isolation system.
11. If control dynamics are included, the control signal to each device should be less than or equal to an absolute maximum of 10 V.
12. Participants of this study are required to submit electronically a complete set of MATLAB files used for their control strategies.

9.1. Matlab and simulink files

Further details, data files, and MATLAB and SIMULINK files can be found at *www.ruf.rice.edu/~nagaraja/baseisolationbenchmark.htm*.

9.2. Note on phase II

In phase II, the participants can compare the results of their controllers with the sample controllers presented by Nagarajaiah and Narasimhan [23] for nonlinear friction isolation system and/or the sample controller presented by Erkus and Johnson [18] in case they consider bilinear elastomeric isolation system such as lead–rubber isolation systems.

10. CONCLUDING REMARKS

A smart base-isolated building benchmark problem with a broad set of carefully chosen parameter sets, performance measures and guidelines to the participants has been defined in this paper. A new nonlinear dynamic analysis program has been developed and made available to facilitate direct comparison of results of different control algorithms.

Participants of this benchmark study can propose different control strategies for the smart base-isolated building problem. Participants can define, evaluate, and report the results for the proposed strategy. The control algorithms may be passive, active or semi-active. In phase I, the participants can compare the results of their controllers with the results of the sample active and semiactive controllers presented by Nagarajaiah and Narasimhan [16, 17] for the nominal linear isolation system. Additionally, they may also compare the results of their controllers with the preliminary skyhook controller presented by Nagarajaiah and Narasimhan [17]. In phase II the participants can compare the results of their controllers with the sample controllers presented by Nagarajaiah and Narasimhan [23] for nonlinear friction isolation system and/or the sample controller presented by Erkus and Johnson [18] in case they consider bilinear elastomeric isolation system such as a lead–rubber isolation system.

ACKNOWLEDGEMENTS

Partial funding provided by the National Science Foundation, CAREER Award 99-96290, and CAREER Award 00-94030, is gratefully acknowledged. The authors would like to thank Professor Bill Spencer, University of Illinois at Urbana-Champaign and Professor W. D. Iwan, CalTech, for their suggestions.

REFERENCES

1. Caughey TK. The benchmark problem. *Earthquake Engineering and Structural Dynamics* 1998; **27**(11):1125.
2. Spencer BF, Dyke SJ, Deoskar HS. Benchmark problems in structural control: part 1—active mass driver system. *Earthquake Engineering and Structural Dynamics* 1998; **27**(11):1127–1139.
3. Spencer BF, Dyke SJ, Deoskar HS. Benchmark problems in structural control: part 2—active tendon system. *Earthquake Engineering and Structural Dynamics* 1998; **27**(11):1141–1147.
4. Ohtori Y, Christenson RE, Spencer BF, Dyke SJ. Benchmark problems in seismically excited nonlinear buildings. *Journal of Engineering Mechanics* (ASCE) 2004; **130**(4):366–385.
5. Yang JN, Agrawal A, Samali B, Wu JC. A benchmark problem for response control of wind excited tall buildings. *Journal of Engineering Mechanics* (ASCE) 2004; **130**(4):437–446.
6. Dyke SJ, Caicedo JM, Turan G, Bergman LA, Hague S. Phase 1: Benchmark control problem for seismic response of cable-stayed bridges. *Journal of Structural Engineering* 2003; **129**(7):857–872.
7. Narasimhan S, Nagarajaiah S, Gavin H, Johnson E. Benchmark problem for control of base isolated buildings. *Proceedings of the 3rd World Conference on Structural Control*, Como, Italy, 2002. CDROM.
8. Narasimhan S, Nagarajaiah S, Johnson EA, Gavin HP. Smart base isolated building benchmark problem. *Proceedings of the 16th Engineering Mechanics Conference*, ASCE, University of Washington, 2003. CDROM.
9. Narasimhan S, Nagarajaiah S, Johnson EA, Gavin HP. Smart base isolated benchmark building. Part I: problem definition. *Proceedings of the 4th International Workshop on Structural Control and Health Monitoring*, Columbia University, 10–11 June, 2004. CDROM.
10. Spencer BF, Nagarajaiah S. State of the art of structural control. *Journal of Structural Engineering* ASCE 2003; **129**(7):845–856.
11. Yang JN, Danielians A. Aseismic hybrid control systems for building structures. *Journal of Engineering Mechanics* (ASCE) 1991; **117**(4):836–853.
12. Yang JN, Li Z, Liu S. Control of hysteretic system using velocity and acceleration feedbacks. *Journal of Engineering Mechanics* (ASCE) 1992; **118**(11):2227–2245.
13. Yang JN, Li Z, Vongchavalitkul S. Stochastic hybrid control of hysteretic structures. *Journal of Probabilistic Engineering Mechanics* 1994; **9**:125–133.
14. Yang JN, Wu J, Agrawal A. Sliding mode control of nonlinear and hysteretic structures. *Journal of Engineering Mechanics* (ASCE) 1995; **121**(12):1386–1390.
15. Park YJ, Wen YK, Ang AHS. Random vibration of hysteritic systems under bi-directional ground motions. *Earthquake Engineering and Structural Dynamics* 1986; **14**(4):543–557.
16. Nagarajaiah S, Narasimhan S. Phase I: controllers for benchmark base isolated building. Part I. *Proceedings of the 4th International Workshop on Structural Control and Health Monitoring*, Columbia University, 10–11 June, 2004.
17. Nagarajaiah S, Narasimhan S. Smart base isolated benchmark building phase I. Part II sample controllers for linear isolation system. *Journal of Structural Control and Health Monitoring* 2006.
18. Erkus B, Johnson EA. Smart base isolated benchmark building. Part III: phase II sample controller for bilinear isolation. *Journal of Structural Control and Health Monitoring* 2006.
19. Alhan C, Gavin HP. Parametric analysis of passive damping in base isolation. *Proceedings of the 16th Engineering Mechanics Conference*, ASCE, University of Washington, 2003. CDROM.
20. Nagarajaiah S, Reinhorn AM, Constantinou MC. Nonlinear dynamic analysis of 3-d-base-isolated structures. *Journal of Structural Engineering* 1991; **117**(7):2035–2054.
21. Nagarajaiah S, Reinhorn AM, Constantinou MC. 3D-BASIS: nonlinear dynamic analysis of three dimensional base isolated structures—part 2. *Report No. NCEER-91-0005*, National Center for Earthquake Engineering Research, State University of New York, Buffalo, 1991.
22. Rosenbrook HH. Some general implicit processes for the numerical solution of differential equations. *Computer Journal* 1964; **18**:50–64.
23. Nagarajaiah S, Narasimhan S. Smart base isolated benchmark building phase II. Part IV sample controllers for nonlinear friction isolation system. www.ruf.rice.edu/∼nagaraja/baseisolationbenchmark.htm
24. MATLAB. The Math Works, Inc., 2000.
25. Yang JN, Agrawal A, Chen S. Optimal polynomial control of seismically excited non-linear and hysteretic structures. *Earthquake Engineering and Structural Dynamics* 1996; **25**(11):1211–1230.
26. Yang JN, Li Z, Wu J, Hsu I. Control of sliding-isolated buildings using dynamic linearization. *Journal of Engineering Structures* 1994; **16**(6):437–444.

